MANOEUVRE DETECTION FOR NEAR-ORBITING OBJECTS

Rafael Vazquez[(1)], Julio C. Sanchez[(1)], Jose M. Montilla[(1)], Jorge Galan-Vioque[(1)], Francisco Gavilan[(1)], Fernando Soler Lanagran[(2)], Javier Rey Benayas[(2)], Francisco A. Rodriguez Lopez[(2)], Jan Siminski[(3)], Cristina Perez Hernandez[(4)]

[(1)] Universidad de Sevilla, Escuela Técnica Superior de Ingeniería, Camino de los Descubrimientos s.n. 41092 Sevilla, Spain, Emails: {rvazquez1, jsanchezm, jmontillag, jgv, fgavilan}@us.es
[(2)] Indra Sistemas, Crta Loeches 9, 28850 Torrejón de Ardoz, Madrid, Spain, Emails: {fsolerl, jreyb, farodriguez}@indra.es
[(3)] Space Debris Office, ESA/ESOC, Darmstadt, Germany, Email: Jan.Siminski@esa.int
[(4)] Centro para el Desarrollo Tecnológico Industrial, C/ Cid 4, 28001 Madrid, Spain, Email: cristina.perez@cdti.es

ABSTRACT

This work outlines and assesses several methods for the detection of manoeuvres from radar data; as it is well-known, radar ranging is a technique well-suited for Low Earth Orbit objects surveillance, providing precise enough ranging accuracy. The main starting assumption is that the manoeuvre is modelled in an impulsive way and that the object under analysis has an orbit known with a sufficient degree of precision. The manoeuvre detector is based on unscented Kalman filtering and reachability analysis of the relative state which correlates its prediction set with the next track from the radar. The methods are being implemented by making use of the space-dynamics library OREKIT and results are presented for simulated scenarios; they will be validated in the near future with real radar data from the Spanish Space Surveillance Tracking and Surveillance Radar (S3TSR), with manoeuvre information and ephemerides obtained from ESA and DLR to assess the results.

1 INTRODUCTION

In the field of Space Surveillance and Tracking (SST), accurate orbital determination and manoeuvre detection is of upmost importance to infer objects' orbital information and their future behaviour, as well as to be able to carry out tasks such as prediction of potential conjunctions with operating satellites, taking avoidance orbital corrections, predicting re-entries, identifying fragmentations or updating orbital elements of known satellites, among others.

Satellites performing unknown manoeuvres pose a challenge when trying to associate the new collected observations (obtained by laser, radar, or by any other means from the SST infrastructure) with the previously known reference orbits (which are stored in SST catalogues). Indeed, one of the main motivations of manoeuvre detection is that it can significantly reduce the number of uncorrelated targets detected by the SST sensors infrastructure. Most of these uncorrelated objects are just known satellites, which have performed unpublished manoeuvres (probably out of sight of the surveillance), in such a way that their new orbits do not match with the predictions.

This work develops several methods for the detection of manoeuvres in Low Earth Orbit (LEO) from radar data, providing some preliminary numerical initial results obtained from simulations. The final aim is to have these algorithm integrated in the S3T Cataloguing System in order to provide routine automatic manoeuvre detection capabilities to the system in the future; thus, as a next step, validation of all the algorithms will be carried out with real tracks from S3TSR [1], the Spanish surveillance radar developed, installed and validated by Indra with the funding of the Spanish Government under the technical and contractual management of ESA on behalf of Centro de Desarrollo Tecnológico e Industrial (CDTI). Manoeuvre information and ephemerides will be obtained from ESA/ESOC and DLR/GSOC to assess the results, for several scenarios.

The structure of this paper is as follows. After this introduction, a literature review is performed for the two main families of methods that can be used to detect manoeuvres, namely: manoeuvre detection filters (based on orbit determination approaches) in Section 2 and reachability analysis-based methods (which compare reachable predicted sets with obtained measurements) in Section 3. The particular implementations selected for this work are presented in Sections 4 and 5, respectively, together with some preliminary results. Finally, in Section 6 numerical results for simulated orbits and radar data are presented. The paper is concluded in Section 7 with some final remarks and future work.

2 MANOEUVRE DETECTION FILTERS

Manoeuvre detection filters (MDFs) employ orbit determination in the process of detecting if some manoeuvre has been performed; they are quite useful, since they are able to correlate new (post-manoeuvre) orbits with previous (pre-manoeuvre) known orbits, thus paving the way to perform orbit determination using quite fewer measures (as compared to a conventional

orbit determination problem). This fact is shown, for instance, in reference [2] where the author compares the accuracy and cost of orbit determination using a manoeuvre detection filter on known flying objects, versus a conventional (cold-started) orbit determination procedure. At its simplest, a manoeuvre detection algorithm relies on Statistical Orbit Determination (SOD) methods (see the reference [3] for a general overview). Very much has been written about the estimation and tracking of spacecraft using radar (or laser) measures, and classical methods like the Batch Least Squares (BLS) method, Extended Kalman Filter (EKF), and the Unscented Kalman Filter (UKF)—or even non-gaussian techniques like the Particle Filter—are well known in the literature.

The problem with traditional methods arises when the target performs unknown manoeuvres in-between the measurements windows, in such a way that the propagators in which the estimation methods are based become too inaccurate (since they do not take into account the manoeuvres) because they have become "overconfident" due to their covariance becoming too small (a filter exhibiting such behaviour is known as a "smug" filter). Thus, a manoeuvring scenario may lead to severe outliers and convergence problems in conventional filtering techniques, but there exist methods to handle these issues and enhance the robustness of these classical algorithms, to avoid divergence problems. For instance, some possible techniques are covariance inflation or fading memory, among others. Additionally, using the filter residuals, a decision logic can be put in place to estimate when a manoeuvre has been performed, in such a way that the filter can be restarted to catch the new post-manoeuvre conditions.

Although the use of these conventional filters is well extended in the literature, recent years have seen the rising of a promising filtering technique for tracking problems known as Multiple Model filters. This scheme (which was in fact originally proposed in 1960) is particularly well suited for problems with highly unstructured uncertainty and is based on a family of elemental filters which can be designed to model different aspects of the system behaviour, together with a probabilistic mixing logic to select the best estimation combining all the outputs of the elemental filters. Manoeuvring target tracking faces two interrelated main challenges: target motion-mode uncertainty and nonlinearity. Multiple-model (MM) methods have been generally considered the mainstream approach to manoeuvring target tracking under motion-mode uncertainty (a good survey about this technique can be found in [4]). The term MMAE (Multiple Model Adaptive Estimation) encapsulates any formulation that considers a multiple model framework consisting of either static models, adaptive models, or both. A MMAE framework allows various models to adapt certain parameters in different ways to account for updates in noise, residuals, or dynamics. There are numerous ways to implement MMAE techniques based on the estimation problem of interest. The approach is general enough to encompass the use of one or several families of filters combined with continuous, discrete or hybrid dynamics (with several possible models) and combine the outputs of multiple models to improve the overall estimate. Of specific interest for manoeuvring spacecraft estimation are MMAE implementations that solve for additional states, adapt noise parameters, and combine the outputs of all models at each time step.

2.1 State of the art on manoeuvre detection filters

Next, a representative sample of MDFs from the literature are analysed with particular focus on the quality and quantity of measurements considered by the authors in experiments or simulations.

Fixed interval smoother for manoeuvre reconstruction

First presented in [5], this algorithm gives a simple approach that uses the orbit determination filters and smoothers directly to provide the estimate of an impulsive manoeuvre. The procedure consists of a sequential filter used to move forward across the manoeuvre and a fixed interval smoother to move backwards across the manoeuvre. The sequential filter serves to process all the tracking data prior to the manoeuvre to provide an optimal pre-manoeuvre state estimate and covariance. The sequential filter then continues across the manoeuvre, adding the uncertainty in the manoeuvre to the velocity sub-matrix of the covariance. Radar data is processed after the time of the manoeuvre until the uncertainty in the state estimate returns to a normal non-manoeuvre condition. At that time, the filter state and covariance are used to initialize the fixed interval smoother, and the smoothing process is run backwards until a time prior to the manoeuvre.

The smoother serves to map information provided by the post-manoeuvre tracking data backwards and provides a smoothed estimate of the post-manoeuvre state. The smoothing process continues across the time of the manoeuvre to yield a smoothed estimate of the pre-manoeuvre state. The difference between the pre-manoeuvre and post-manoeuvre smoothed states may now be extracted as the estimate of the manoeuvre. The pre-manoeuvre and post-manoeuvre smoothed covariance matrices are used to compute the uncertainty associated with the estimate of the manoeuvre. It is noteworthy that no additional states are added to the estimation process and that this solution can be done in the process of normal orbit analysis.

As drawback of this method (which may be considered a "naïve" method proposed early in the history of MDFs),

it is assumed that one can quickly obtain a good state estimate after manoeuvre has passed. However, this might not be the case because of filter convergence problems. Nevertheless, it has the advantage of being flexible enough to use with any single or multiple orbit determination filter. In addition, the authors provide real examples which do not differ much from the scenario considered in this work (LEO satellites and radar data).

Variable structure estimators

This approach is proposed in reference [6], where a manoeuvre detection metric is used to design an estimator with an additional manoeuvre observer module, the so-called "variable structure estimator." In this scheme an EKF is used together with a manoeuvre observer (which is in turn triggered when the manoeuvre detection metric reaches a certain threshold). Then, the manoeuvre observer estimates the manoeuvre acceleration, and sends that information to the EKF, which takes into account the estimated acceleration to improve the orbit propagation in its algorithm. Note that this approach can be easily adapted to a BLS- or UKF-type of filter. The "manoeuvre observer" is based on a simple first-order observer, which produces an estimation of the acceleration to be fed back to the EKF. The approach is attractive because of its simplicity; however, the main disadvantage of the proposed MDF is that it assumes that numerous radar measurements are available so that manoeuvres are always observed. Since, in the scenarios considered in this work, there are long time gaps in-between measurements (typically, 12 or more hours), one would need to discretize the trajectory at many times (candidates to be the time of application of the manoeuvre).

Joint kinematic/dynamic filters

This approach is proposed in [7] and consists of two filters (EKF, UKF, or other types) running in parallel. The first filter is a traditional orbit determination Kalman filter. The second filter is a kinematic filter and utilizes some representative random processes (with design parameters) to describe the orbital motion. While the detailed motion is not captured at all, the changes caused by orbital manoeuvres can be captured by those flexible random processes.

Note that the dynamic model is used as the main, primary filter, since it produces much more detailed orbit predictions, whereas the kinematic model helps to detect manoeuvres. The manoeuvre detection scheme is based on changes of the estimated semi-major axis from the kinematic model. In addition, the dynamic model filter can help to detect manoeuvres based on residuals' behaviour (similar to the metric proposed in [6]).

The approach becomes more complex due to the necessity of tuning an efficient kinematic model for the scenarios. In addition, while the reference does not assume continuous measurements, the simulations included therein consider three radars for a satellite in a Medium Earth Orbit. Thus, it is unclear if this approach can be adapted to the scenarios considered in this work, with long time gaps in-between measurements. However, the idea of using a purely statistical model (always as part of a batch of filters) may have some merits to be explored in the future.

Filter-through and manoeuvre reconstruction

This approach, extracted from [8] and [9], is based on a procedure to estimate a post-manoeuvre orbit. The results presented therein show that a filter-through Interacting Multiple Model orbit determination filter (EKF or UKF) can converge on a post-manoeuvre orbit with similar performance to Initial Orbit Determination approaches, based on multiple filters running with different levels of covariance inflation. Note that this filter-through would only kick-in if a manoeuvre has been detected, with detection based on residual analysis following along the lines of [6]. Once the post-manoeuvre orbit is known with a certain degree of accuracy, to reconstruct a single manoeuvre, the most general approach is to propagate the pre-manoeuvre orbit forward in time and the post-manoeuvre orbit backwards in time. Next, determine the time when the orbits intersect, touch, or come closest together (minimum separation distance). This instance is the time of the manoeuvre, and the difference of the velocity vectors is an approximation of the impulsive manoeuvre ΔV. In addition, with some knowledge of the post- and pre-manoeuvre orbits, it is possible to simplify the procedure (e.g., if the orbits are coplanar or there is a plane change).

3 REACHABILITY ANALYSIS

In this section the idea of Reachable Sets (RS) and their analysis (Reachability Analysis, RA) is introduced, as well as their relationship with control and estimation of systems. This background material constitutes the foundational framework for Section 5.

Citing [10], "*the concept of reachability is central to Space Situational Awareness (SSA)*," which underscores the interest of this concept for the present work. Reachability Analysis deals with the study and applications of Reachable Sets, which are defined as follows: given a system that evolves from an initial condition (or set of initial conditions), and possibly has some control inputs, the reachable set is the set of states at which the system can arrive (i.e., the states that can be reached) at a given time.

To more formally define a RS, start by considering a dynamical system, which is assumed to be defined with a differential equation $\dot{x} = f(t, x, u)$. In the equation, x is the state (for instance, position and velocity) of dimension n (6 in our case), t the time, and u a possible control input (which might represent a manoeuvre) for some sufficiently regular function f (in orbital

mechanics, f might be Kepler's equation, Gauss' variational equations, the relative dynamics equation or any other differential equation used for orbit propagation). Traditionally, one solves such a differential equation with an initial condition $x_0 = x(t_0)$ given at time t_0 and a certain control input $u(t)$, thus obtaining a trajectory $x(t)$ valid for $t \geq t_0$. Based on these solutions one can define the state trajectories flow, $x(t) = \varphi^{t,t_0}(x_0, u)$ which includes all the dependencies of the solutions.

A Reachable Set (RS) is defined as follows. Consider an initial set (instead of a point) of initial conditions at t_0, and denote it by Ω_0. Consider the set of all possible actuations U. Then, the RS from Ω_0 at time t, denoted as $\Omega(t)$, is defined (assuming there are no collisions or singularities for the flow) as

$$\Omega(t) = \{x \in \mathbb{R}^n : x = \varphi^{t,t_0}(x_0, u), x_0 \in \Omega_0, u \in U\} \quad (1)$$

Such description is very convenient to characterize the state evolution over time starting from uncertain initial conditions or unknown control inputs, or to analyse what states can be (or not be) reachable with a particular control law. The technique has been used, for instance, in the context of rendezvous of spacecraft [11]. The idea has many applications. For instance, one of the main applications of RA is in the area of safety for trajectories of vehicles (which could be aircraft or spacecraft); if there is a dangerous zone (for instance, where collisions could happen), one way to ensure safety is to enforce that the RS is always away from the dangerous zone.

Even in the linear case, the dependence on the control set U can make the computation of these sets quite difficult, with ellipsoids being a classical choice for representations, see e.g. [12].

If the dynamics are non-linear (as is the case in orbital mechanics), a state transition matrix is not available, and therefore the computation of reachable sets becomes challenging and highly intensive in computational terms [12], as a very large number of state propagations are required. One of the preferred representations of RS is based on zonotopes [13], which is a region spanned from the linear combinations of a set of N vectors, namely $\sum_1^N \alpha_i \vec{v_i}$, but limiting the coefficients α_i between 0 and 1. However, the approach taken in this document is more aligned with the uses of RA in the context stochastic control theory (see for instance [14]); if one considers that the differential equation is to be interpreted in a stochastic sense, with initial conditions given not deterministically but rather as a certain initial probability distribution, then one can consider as the initial set Ω_0 a confidence region of the initial probability distribution (which means that most initial conditions are contained in Ω_0 with probability p—the degree of confidence of the region—) then the RS, $\Omega(t)$, will also correspond to a confidence region.

Computing reachability sets in the nonlinear case is extremely challenging, since, in principle, with six states (three pertaining to position and three to velocity) that may have some degree of uncertainty, one would require to propagate the boundary of a six-dimensional closed manifold, as well as the probability distribution function inside of it. Thus, in this project a particle-based approach is applied (very much in the spirit of the Montecarlo method), in which one samples the initial confidence region Ω_0, (following the probability distribution of the initial conditions), to obtain approximations of the sets Ω(t) and the evolved distribution function. Since a large number of particles (trajectories) need to be propagated, two main ideas help to reduce the computational burden.

The use of differential algebra techniques such as Taylor expansion over an initial condition can be employed in order to obtain reachable sets from an initial condition set in a reasonable amount of time (see [15] or [16]). Notice that this in fact represents a higher-order approach than the classical propagation of covariances (linear approach), that rely on Jacobians and the assumption that Gaussian distributions keep being Gaussian (which is only true under linear transformations). This "Gaussianity" hypothesis quickly begins to fail since the nonlinearity of the propagation "distorts" the distribution, making it lose its shape [10]. Thus, better/more accurate results can be expected from this approach particularly if not many measurements are available and propagation times are not short, but rather of the order of hours, as it is in the case of this project.

Nothing has been said so far about the presence of u in the differential equation. If it is set to zero, then the RS represents the possible future states of the system when no control is applied (in the context of the project, in the absence of manoeuvres); then it does not differ at all from basic stochastic differential equations theory (this is, propagation of uncertainties). Obviously, if there exists some control u then the results change. The reference [10] considers the problem of computing the maximal RS subject to control being equal or less than some given constraint and solves the problem for relative orbital mechanics (in the absence of perturbations) by applying optimal control, bounding the result by ellipsoids.

In addition, one of the most interesting applications to SST of reachability analysis is the problem of object correlation. Oftentimes, new measurements of space objects that have manoeuvred need to be correlated with previously known orbits, however there might be several candidates and one needs to choose which one to associate with the new measurement. Looking at the literature, this problem has indeed received considerable attention in the last years. There are a number of metrics that can be used such as the Mahalanobis distance [17] and techniques that can help when several measurements are present, such as the use of attributables [18] (see also

[19]), but these do not explicitly take into account the possibility of manoeuvring objects, which however is critical since (citing [19]), small fuel expenditures at specific points in an orbit can produce outsized state discrepancies. This problem is tackled in [20] and [19] computing (by means of optimal control) the minimum possible manoeuvre that connects the previous orbit with the new measurements. In [21] this optimal control approach is compared with the use of historical data, which is found more accurate when available (at least for the GEO example considered in that paper) and if the manoeuvres are predictable. These ideas are used in this work to develop manoeuvre detectors.

4 A MANOEUVRE DETECTION FILTER BASED ON UKF

To decide which filter to develop for this work, it is important to take into account that the S3TSR [1] is the only source of measurement data for this project. This implies that objects will have long windows without observation in-between, from about half a day up to 3 days, and then a batch of observations will become available. Therefore, designs relying on a large number of measurements and/or frequent measurements are not implementable. The scheme of [6] is adapted, with manoeuvre detection based on residue analysis. As for the choice of the filter type itself, the UKF seems to be the superior choice.

Whereas EKFs have been widely used in the past for estimation purposes in nonlinear settings, when dealing with severe nonlinearities, its accuracy might be compromised, since the "Gaussianity" hypothesis in which the EKF is based might be quite far from reality. Trying to overcome this drawback, the UKF was developed, to provide good results even for nonlinear systems while preserving Gaussian models. The UKF is based on the "unscented transformation" first proposed by Julien and Uhlmann [23] and later improved by Wan and Van Der Merwe [24] to compute the first two moments of the probability density distribution of a random variable given by some transformation $y = h(x)$, assuming that the mean and the covariance of the variable x are known. The idea behind the unscented transformation is that a set of points x^i (called sigma-points) can be found in the domain of x, in such a way that transformed sigma-points $y^i = h(x^i)$ can be used to accurately approximate the exact mean and covariance of y (by using a predefined set of weights).

4.1 UKF algorithm

Considering a system with n states, given by the following process and observation equations

$$\dot{x} = f(x,t), \tag{2}$$

$$y = G(x,t), \tag{3}$$

and a set of weights to estimate the mean and the covariance (denoted by w_m^j and w_c^j respectively, for $j = 1, \dots, 2n+1$), together with a tuning parameter κ (see the reference [2] for a description of the weights and the tuning parameter values), the UKF algorithm is (see [2] for details on the different steps):

1. Start from the previous estimate of the state and the covariance of its error ($\hat{x}_0$ and $\hat{P}_0$).
2. Compute the sigma-points of the unscented transformation.
3. Propagate all the sigma points using numerical integration.
4. Compute the weighted mean and the covariance matrix of the transformed sigma-points.
5. Read the next observation.
6. Transform the sigma-points (using the observation equation) and calculate the predicted observation, the residuals, and the observation covariance.
7. Calculate the predicted cross-correlation covariance and the residuals.
8. Compute the Kalman gain and update the estimate of the state.
9. Return to step 1 and continue propagating.

4.2 Manoeuvre detection

Finally, the filter can be adapted to estimate the presence of manoeuvres. Thus, in the 7th step of the UKF's algorithm, a manoeuvre prediction metric can be included, which reads:

$$\Psi_i = \nu_i^T S_i^{-1} \nu_i, \tag{4}$$

with ν_i being the residuals and S_i^{-1} the observation covariance. This term can be used to estimate model mismatches (due to manoeuvres), and then trigger other manoeuvre detection algorithms.

4.3 Smoothing

In the scenario considered in this work, measurements from the radar come in batches of 5-20 measurements with long intervals in-between them (hours). Any filter developed for this situation has to take this scenario into account. While the BLS approach is simultaneous in nature, the KF approaches (EKF/UKF) will process the measurements sequentially, in the order they were obtained. Thus, if a KF scheme is used, after the conclusion of the filtering algorithm, this is, after a batch of measurements has been processed, the output of the filter can be improved via a backwards *smoother*. This additional algorithm propagates the filter backwards in time, starting from the last measurement in a batch, up to the first one, modifying estimates accordingly (see [2] for details). It is well-known that smoothers provide considerable improvement for orbit determination. As future work longer smoothing intervals will be

considered (e.g., propagating backwards up to the previous radar batch).

4.4 UKF Process and measurements

As a first step, the UKF must be tuned to work correctly in the absence of manoeuvres. The UKF process is an orbit propagator implemented in OREKIT [25]. The radar measurements are range, range rate, azimuth and elevation. The radar accuracy on each measurement is as follows: Range: 7 m (1-σ); Azimuth / Elevation: 0.3-0.5º (1-σ); Range rate: 0.4 m/s (1-σ). In terms of distance, for LEO (600 km range), the angular measurement error translates into a distance error of about 5.24 km. Consequently, radar angular accuracy is poor compared to range measurements. Thus, only range and range rate measurements are considered as the filter's inputs.

4.5 Process noise estimation

The UKF algorithm requires the process noise covariance as an input. This quantifies mismatches with respect to the real process. Consequently, it is a key factor in the filter as it will balance the credibility of the process with respect to the measurements. In any case, the process covariance is unknown, as its exact knowledge would imply perfect modelling, and has to be tuned. Initial covariance needs also to be estimated to be as realistic as possible [26]. In [27], the state noise compensation technique described next is recommended as a good practice for navigation filters and has been adopted.

Denote by LVLH a Local-Vertical, Local-Horizontal frame. Assuming LVLH velocity error as Gaussian white noise with covariance

$$\mathrm{Q_{LVLH}} = \begin{bmatrix} q_x & 0 & 0 \\ 0 & q_y & 0 \\ 0 & 0 & q_z \end{bmatrix}, \qquad (5)$$

then, the transformation to inertial coordinates can be made using the rotation matrix R_{LVLH} which transforms LVLH coordinates to the inertial frame

$$\mathrm{Q} = \mathrm{R_{LVLH}} \mathrm{Q_{LVLH}} \mathrm{R_{LVLH}^T}. \qquad (6)$$

Dividing the elapsed time between radar batches of measurements (tracks) in increments Δt, where the inertial orientation of the LVLH frame is assumed constant, the full state inertial covariance grows during an interval k as a second-order random walk model:

$$\mathrm{S}_k = \begin{bmatrix} \mathrm{Q}\Delta t^3/3 & \mathrm{Q}\Delta t^2/2 \\ \mathrm{Q}\Delta t^2/2 & \mathrm{Q}\Delta t \end{bmatrix}, \qquad (7)$$

and then process noise covariance estimation is

$\mathrm{S} = \sum_{k=1}^{N} \mathrm{S}_k$, for filter calls between tracks,

$\mathrm{S} = 0_{6\times6}$, for filter calls within a track.

Within a track, where measurements are obtained every few seconds, the process mismatch is negligible.

4.6 UKF preliminary testing results

Numerical results are shown in order to justify the chosen implementation. The considered scenario is the LEO satellite Sentinel-1A (with orbital elements taken from public TLEs and assumed precise, propagated with second-order gravity harmonics and drag) between 16:00:00 08/07/2015 – 16:00:00 12/07/2015. The radar measurements are obtained geometrically. The following results assume a model mismatch in drag, with $C_D = 2.2, S = 10\ m\text{^}2$ the real drag coefficient and exposed surface and $C_D = 2, S = 9.5\ m\text{^}2$ the assumed ones. The LVLH acceleration errors for (5) are

$$q_x = 10^{-9} m^2 s^{-3}, q_y = q_z = 5 \cdot 10^{-10} m^2 s^{-3},$$

where more noise has been assumed in the tangential direction. The discretization time period is taken as $\Delta t =$ 10 min. A comparison with a simulation assuming a null process covariance noise is shown in Figure 1 (red dots indicate the mismatch between measurements and the predicted state after the filter update).

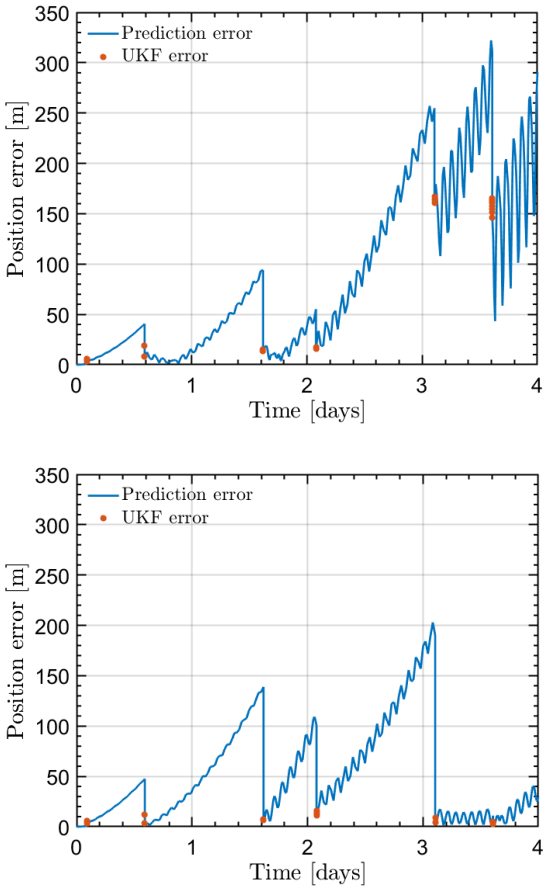

Figure 1. Position error without process noise (top) and estimating process noise (bottom).

In the results, the initial covariance is assumed small and

with a realistic shape (obtained from running the filter for a few days); using a diagonal shape resulted in a much poorer performance of the filter.

For manoeuvre detection, the metric (4) was adapted as

$$\Psi = \frac{1}{n}[\mathbf{v}_1^T \dots \mathbf{v}_n^T] \begin{bmatrix} \mathbf{S}_{z,1} & \cdots & \mathbf{0}_{2x2} \\ \vdots & \ddots & \vdots \\ \mathbf{0}_{2x2} & \cdots & \mathbf{S}_{z,n} \end{bmatrix}^{-1} \begin{bmatrix} \mathbf{v_1} \\ \vdots \\ \mathbf{v_n} \end{bmatrix}, \quad (8)$$

where the subindex refers to each radar block measurement of range and range-rate. As the detection method is based on finding significant discrepancies between the predicted orbit and the actual one, the residuals are computed prior to smoothing.

A proof of concept is shown for the same scenario with a manoeuvre. The manoeuvre start is 00:34:58 11/07/2015 and ends at 00:35:24 11/07/2015 with a constant acceleration of $u = [0.31 \cdot 10^{-2}, -0.35 \cdot 10^{-3}, 0.37 \cdot 10^{-5}] m/s^2$ in the LVLH frame.

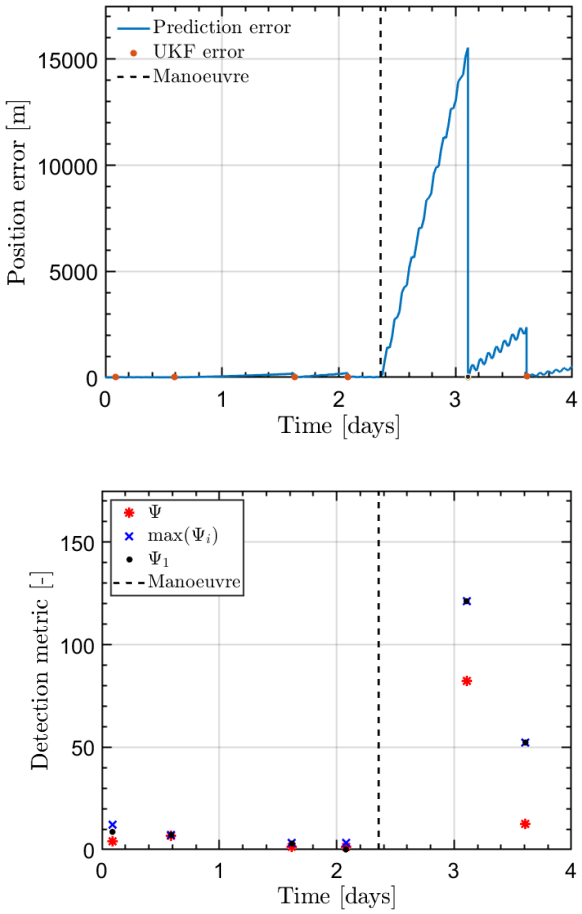

Figure 2. UKF position error with manoeuvre (top) and detection metrics comparison (bottom).

In Figure 2, the UKF demonstrates its capability to recover the orbit after the manoeuvre is applied. Moreover, a comparison of other possible detection metrics is also shown. The other explored alternatives are to take the maximum Ψ_i of the track or the one associated to the first block of radar measurements Ψ_1.

5 REACHABILITY-BASED MANOEUVRE DETECTION ALGORITHMS

In this section, RA as outlined in Section 3 is applied to the specific problem of Manoeuvre Detection. Thus, the starting inputs are the precise orbit of the objects (pre-manoeuvre) and the radar measurements and the outputs are the probability of a manoeuvre having happened.

As a first step, the theory of attributables (see [18] and [19]) is introduced; it allows to "compress" several measurements into a single, higher-quality measurement, fitting a batch of measurements into a single polynomial expression whose order needs to be determined.

Next, two algorithms are explained; the first is based on comparing the range-range rate attributable obtained from measurements with the one obtained from the initial uncertain orbit, by means of confidence regions and the Mahalanobis distance, which is a measure of the distance between a point P and a distribution (see [17]).

The second algorithm is based on the use of optimal control theory. Following the ideas of [20] and [19] one can compute by means of stochastic optimal control a distribution of the ΔV that connects the uncertain orbit with the measurement. This distribution can then be used to obtain the likelihood of a manoeuvre having been performed.

5.1 Attributables

In order to condense the information of all measurements in each track the strategy of the attributables has been used [19]. A radar provides range, range-rate, elevation and azimuth, that, coupled with the chosen reference epoch, form the attributable

$$\mathcal{A} = \{t, \rho, El, Az, \dot{\rho}\}. \quad (9)$$

Fitting the information of the observables independently is one option, but it is possible to improve the uncertainty of the resulting virtual measurement if one incorporates the definition of range-rate into the modelling, so that it shares the parameters with the range:

$$\rho(t) = \rho_0 + \rho_1 t + \rho_2 \frac{t^2}{2!} + \cdots + \rho_n \frac{t^n}{n!}, \quad (10)$$

$$El(t) = El_0 + El_1 t + El_2 \frac{t^2}{2!} + \cdots + El_n \frac{t^n}{n!}, \quad (11)$$

$$Az(t) = Az_0 + Az_1 t + Az_2 \frac{t^2}{2!} + \cdots + Az_n \frac{t^n}{n!}, \quad (12)$$

$$\dot{\rho}(t) = \frac{d\rho(t)}{dt} = \rho_1 + \rho_2 \frac{2t}{2!} + \cdots + \rho_n \frac{nt^{n-1}}{n!}. \quad (13)$$

In the above expression, the origin of time is at the middle

time of the track.

This method manages to average out noise and reduce the standard deviation of the virtual measurement. Following the nomenclature in [19], the set of equations that allows to solve the parameters in the sense of least-squares is:

$$m = \begin{bmatrix} \rho_* \\ El_* \\ Az_* \\ \dot{\rho}_* \end{bmatrix} = \mathrm{A}_{SYS}\mathrm{p} + \upsilon = \begin{bmatrix} \mathrm{A} & 0 & 0 \\ 0 & \mathrm{A} & 0 \\ 0 & 0 & \mathrm{A} \\ \mathrm{A}_{\dot{\rho}} & 0 & 0 \end{bmatrix} \begin{bmatrix} \hat{\rho} \\ \widehat{El} \\ \widehat{Az} \end{bmatrix} + \upsilon, \quad (14)$$

Where m contains the measurements of all observables, p are the parameters that one wants to calculate, and the matrices A and $\mathrm{A}_{\dot{\rho}}$ have, respectively, coefficients found from the attributable time-varying formula for (ρ, El, Az) and $\dot{\rho}$ respectively. The error $\boldsymbol{\upsilon}$ follows the distribution of the measurements. Then the problem to solve is posed as weighted least-squares as follows

$$\min_{\mathrm{p}} \upsilon^T \mathrm{W} \upsilon = \min_{\mathrm{p}} (m - \mathrm{A}_{SYS}\mathrm{p})^T \mathrm{W} (m - \mathrm{A}_{SYS}\mathrm{p}), \quad (15)$$

where the solution is well-known:

$$\mathrm{p} = (\mathrm{A}_{SYS}^{\mathrm{T}} \mathrm{W} \mathrm{A}_{SYS})^{-1} \mathrm{A}_{SYS}^{\mathrm{T}} \mathrm{W} m. \quad (16)$$

This method manages to average out noise and reduce the standard deviation of the virtual measurement. The weighting matrix W is chosen to be the inverse of the covariance matrix of $\boldsymbol{\upsilon}$, $\Sigma_{\boldsymbol{\upsilon}}$, thus the attributable parameters covariance matrix is:

$$\Sigma_p = (\mathrm{A}_{SYS}^{\mathrm{T}}\, \Sigma_{\upsilon}^{-1}\, \mathrm{A}_{SYS})^{-1}. \quad (17)$$

This allows to know how good the virtual measurement $\alpha(t)$ for a given observable with parameters p_i is going to be at any point of the fit:

$$Var[\alpha(t)] = \sum_{i,j} \sigma_{ij} \frac{t^i t^j}{i!\, j!}\,. \quad (18)$$

This expression, if evaluated at the epoch of the attributable ($t = 0$), gives σ_{00}, the covariance of the first parameter. The elements σ_{ij} (the coefficients of Σ_p) are sufficient to provide the covariance matrix of the complete attributable ($\Sigma_{\mathcal{A}}$) at the epoch without further processing, so that any information derived from $\mathcal{A}$ will have uncertainty information, such as the position in inertial coordinates.

A test track with radar standard deviations $\sigma_\rho = 30\ m$, and $\sigma_{\dot{\rho}} = 10\ m/s$ has been used for an example of range attributable, zoomed around the centre, as it is the point chosen for the virtual measurement, in Figure 3. The uncertainty is mitigated with a noticeable reduction in the standard deviation by 40% (in the case of the range rate, the reduction is by 80%, a consequence of the methodology used for the definition of the range-rate attributable.

In addition, one can estimate the azimuth and elevation rates and use it to perform a simple Initial Orbit Determination. However, notice that this would give a rather inaccurate approximation for an orbit passing through the measurement (one cannot expect to perform a good IOD with such a short observation arc), and therefore it is not pursed in this work.

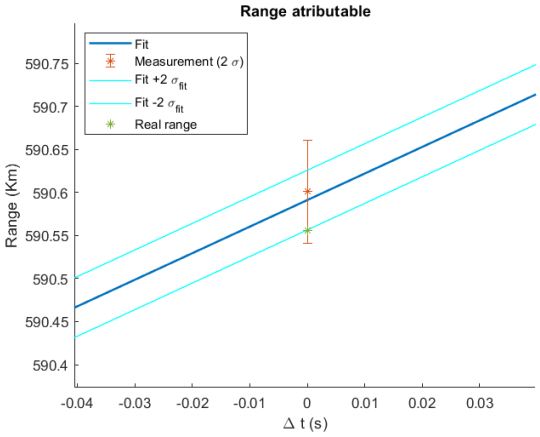

Figure 3. Range attributable and reduction of error

5.2 Algorithm 1: Comparison of real and projected attributables

Applying the ideas of Section 5.1, from the measurements at times t_i one can obtain the virtual values of range, range-rate, azimuth and elevation at the middle of a track, namely $(\rho_0, Az_0, El_0, \rho_1)$ as well as the associated uncertainty in the form of a covariance matrix Σ. This is denoted as the attributable.

The following algorithm is used to obtain a "projected" (or predicted) measurement from the initial value of the reference orbit, which is assumed to follow a certain known distribution:

- Sample the PDE of the initial condition obtaining m sample points. Denote these as x_{0j} for $j = 1, \ldots, m$. The set of initial conditions Ω_0 is then approximated by these points.
- Propagate the sampled points using an OREKIT propagator up to time t_f. Taylor differential algebra methods can be used to greatly speed up this computation, at the price of a lengthy initial calculation [28]. Thus, one obtains m trajectories $x_j(t)$.
- Projected values at the attributable time t_i are obtained as a cloud of points $\mathrm{x}_j(t_i)$, with the density of points giving an approximate measure of the probability associated to the real trajectory.
- Now for each sampled orbit, one can compute the measurements at t_i, obtaining a "cloud" of measurements, from which one can obtain its mean $(\widehat{\rho_0}, \widehat{Az_0}, \widehat{El_0}, \widehat{\rho_1})$ as well as the associated

uncertainty in the form of a covariance matrix $\hat{\Sigma}$. This is denoted as the projected measurement (in the sense that it is the attributable value one would expect given the starting distribution of the initial condition).

- Finally, the attributables and projected measurements can be compared. If no manoeuvre has been performed, one would expect that both values should somewhat agree. To formulate this more precisely, define:

$$\begin{bmatrix} \Delta\rho_0 \\ \Delta El_0 \\ \Delta Az_0 \\ \Delta\rho_1 \end{bmatrix} = \begin{bmatrix} \rho_0 \\ El_0 \\ Az_0 \\ \rho_1 \end{bmatrix} - \begin{bmatrix} \widehat{\rho_0} \\ \widehat{El_0} \\ \widehat{Az_0} \\ \widehat{\rho_1} \end{bmatrix}, \Delta\Sigma = \Sigma + \hat{\Sigma}. \quad (19)$$

- Then, if there is no manoeuvre, one would expect that, under an assumption of normality, $(\Delta\rho_0, \Delta Az_0, \Delta El_0, \Delta\rho_1)$ should belong to a normal distribution of zero mean and covariance $\Delta\Sigma$. This can be checked either by computing confidence regions or equivalently through the Mahalanobis distance, as briefly explained next.

Use of confidence regions and Mahalanobis distance.

For a multivariate normal distribution with mean m and covariance matrix Σ, the p-level confidence ellipsoid (this is, the ellipsoid containing with probability p samples from the distribution) is given by

$$(x-m)^T\Sigma^{-1}(x-m) \leq \chi_n^2(p), \quad (20)$$

where $\chi_n^2(p)$ is the inverse cumulative distribution function of the chi-square distribution with n degrees of freedom (the dimension of the vector x), evaluated at the probability value p. Similarly, the Mahalanobis distance is a measure of the distance of a point x from a distribution. It is unitless, scale-invariant and takes into account the correlations of the distribution. Concretely, if the distribution has mean m and covariance matrix Σ the Mahalanobis distance (MD) is computed as

$$MD = \sqrt{(x-m)^T\Sigma^{-1}(x-m)}\,. \quad (21)$$

In particular if the distribution is a multivariate normal, then the MD has a chi-square distribution with n degrees of freedom; thus, it is equivalent to the use of confidence ellipsoids. This property can be used to compute probabilities of manoeuvre.

Next, an example is shown where the comparison of real and projected attributables is carried out for two cases: one example with manoeuvre and one without. Figure 4 shows that the confidence intervals and MD are able to discriminate the manoeuvred case from the non-manoeuvred one, at least for a simple basic simulation, using range and range rate. Further testing to fix a threshold in the MD to determine if a manoeuvre has been performed or not, as well as how to find the probability of manoeuvre, is done in Section 6.

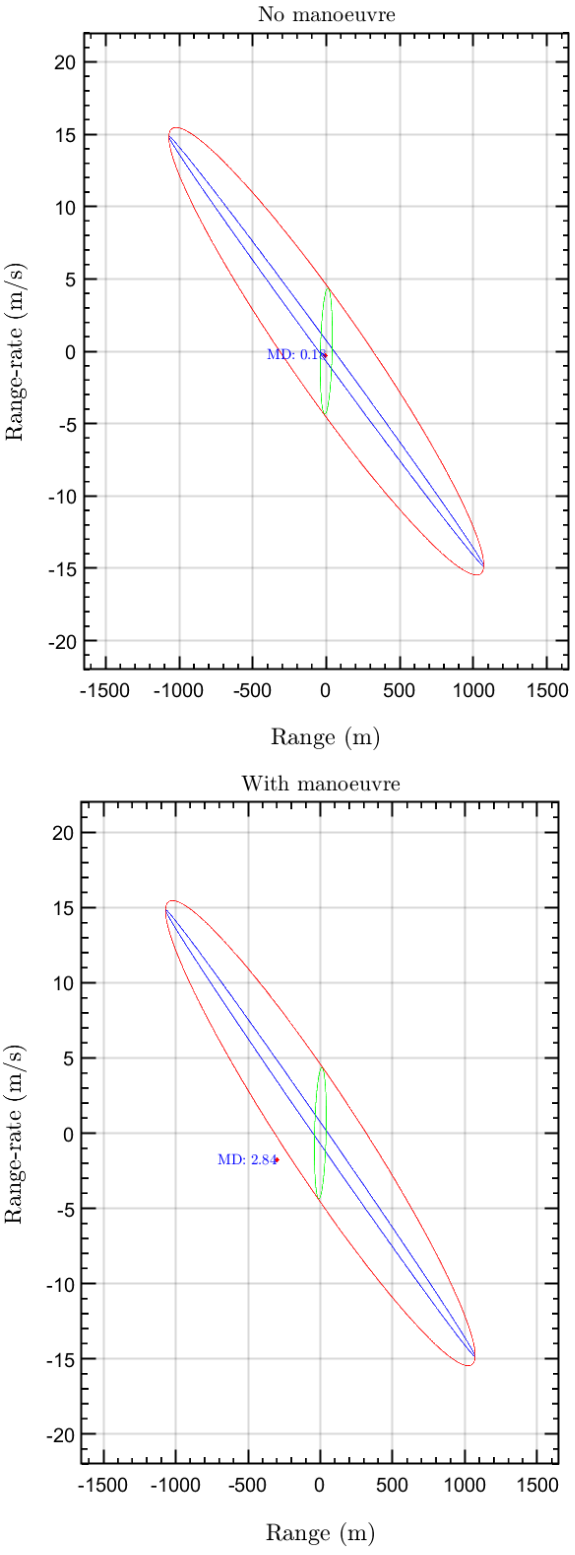

Figure 4. Confidence intervals (90%) and Mahalanobis distance, considering only range and range-rate, without manoeuvre (top) and with manoeuvre (bottom). The green ellipse represents the measurement uncertainty, the blue one the orbit uncertainty, and the red one the total uncertainty.

5.3 Algorithm 2: use of optimal control to compute a ΔV measurement of distance.

As a more sophisticated alternative to the Mahalanobis distance ([20], [21]) one can compute by means of stochastic optimal control a distribution of the minimum ΔV that connects the uncertain orbit around it. This distribution can then be used as a metric to obtain the likelihood of a manoeuvre having been performed. The optimal control problem is posed as follows:

$$Min_u \int_{t_0}^{t_f} u^T(t)u(t)\,dt$$

$$s.t. \quad x'(t) = f(x(t), u(t), t)$$

$$x(t_0) = x_0,$$

$$h\left(x(t_f)\right) = [\rho\ \dot{\rho}]^T$$

In the above optimal control problem, the initial point is known from the precise orbit whereas the function h at the final point represents the function relating position and velocity with range and range-rate (the most precise measurements) which should take the value obtained with attributables as explained in Section 5.1. The function f represents the orbital dynamics, including any desired perturbation. The selected functional would represent the energy of the manoeuvre acceleration, which is less problematic than its L_2 norm from a numerical point of view (which could be also replaced by the Huber approximation [20]; this is left for future iterations). It is well known from the literature that the real ΔV is bounded by the square root of this quantity.

The problem is solved with CasADi [29], an open-source solver for MATLAB, with a multiple shooting method discretizing the orbital dynamics in N time intervals; for each of these, since impulses are small, the orbital dynamics is replaced with a linearized model obtained from OREKIT (computing the State Transition Matrix), with the discrete ΔV's applied at the beginning.

As a first step, the problem has been solved in a deterministic way. Since the solution is fast (seconds or less), to incorporate the stochasticity of the problem (both in initial orbit and measurements), a Monte Carlo algorithm has been implemented as a simple solution, albeit rather time-consuming. Figure 5 shows the obtained cumulative empirical distribution of ΔV (1000 samples) for two cases (with and without manoeuvre) and gives a proof of concept of how this approach can discriminate measurements from orbits with or without manoeuvres. It is clear that the distribution without manoeuvre is "smaller" than the one with manoeuvre.

6 NUMERICAL SIMULATIONS

Several OREKIT-based simulators both for the manoeuvres and for the radar observations have been developed. They provide realistic (though not accurate) testing examples. They are very useful to tune and validate the different algorithms and filters. Starting point are generated from public TLEs.

These are used to define reference orbits with propagators including J2 and aerodynamic drag, as explained in Section 4.6.

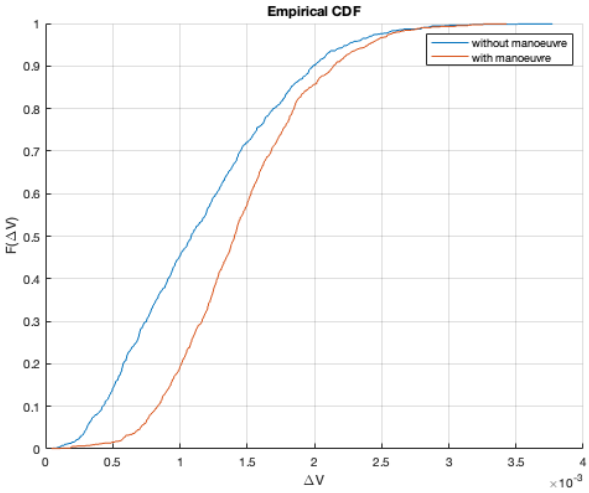

Figure 5. Empirical distribution of impulse computed from the stochastic optimal control problem (obtained from 1000 samples).

The algorithms, besides the model mismatches explained in that section, start from initial conditions within the expected limits of error of the real precise orbits (meters). Two main scenarios, respectively based on Sentinel 1A and Swarm C, are considered. A tangential manoeuvre is simulated, maintaining a constant acceleration of 10^{-3} m/s^2 and characterized by the following fields:

- Manoeuvre intensity (regulated through the duration): low (5 seg) / medium (30 seg) / high (120 seg).
- Manoeuvre location with respect to a radar track: 2 h / 6 h / 12 h.
- The Sentinel-1A scenario spans from 00:00:00 18/08/2020 to 00:00:00 22/08/2020. The manoeuvre starts at 18:25:00 20/08/2020.
- The Swarm C scenario spans from 00:00:00 14/07/2020 to 00:00:00 20/07/2020. The manoeuvre starts at 12:30:00 17/07/2020.

Thus, combining all these factors, one gets 18 simulation scenarios to try to analyse the influence of these factors for the algorithms. Due to space limitations, only Sentinel 1-A results are presented, and some comments given on the Swarm C result.

6.1 UKF Results.

The result without manoeuvre is presented in Figure 6

whereas the manoeuvred case is given in Figure 8. The value of Ψ which should help in detecting manoeuvres is given for all cases in Table 1.

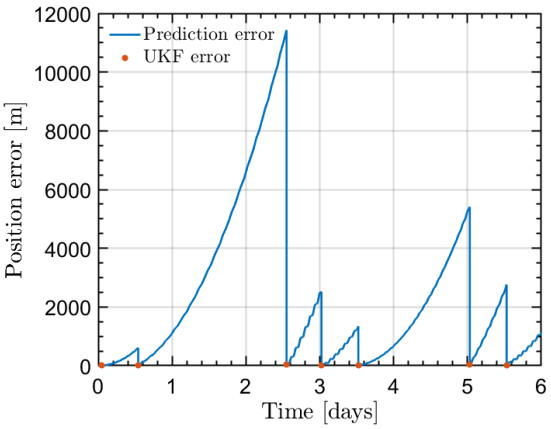

Figure 6. Position error for Sentinel-1A with respect to "real" orbit without manoeuvre. Red dots indicate the mismatch between measurements and the predicted state after the filter update.

Case / Ψ	Pre-man. Max.	Post-man. Max.
No manoeuvre	11.03	4.592
low -2 h	11.03	3.160
low -6 h	11.03	4.667
low -12 h	11.03	7.104
medium -2 h	11.03	4.612*
medium -6 h	11.03	5.905
medium -12 h	11.03	7.254
high -2 h	11.03	501.3*
high -6 h	11.03	58.51*
high -12 h	4.435	75.89

Table 1. Maximum value of detection metric before and after Sentinel-1A out-of-plane manoeuvre. The asterisk indicates that the maximum arises after the first post-manoeuvre track (i.e., at a later batch of measurements).

The results conclusions are as follows:

- The filter takes some time to stabilize. This is probably due to the incorrect initial covariance. Since in real scenarios the covariance will not be perfectly known this can be expected.
- The filter is working correctly in all cases, since the measurements are scarce it is unavoidable that the position errors grow, however, they are mitigated at each measurement.
- Manoeuvres induce large errors after they happen, since the dynamic from the manoeuvres is unmodelled and therefore unaccounted for in the process covariance. The largest the manoeuvre the larger the error and the more it takes to recover from it.
- The value of Ψ is indicative of the presence of a manoeuvre only in medium and specially in high-intensity cases. Low-intensity manoeuvres are indistinguishable from process noise.
- The distance to the radar measurement does not seem to have much influence in the value of Ψ.

In the Swarm C case (not shown), the value of Ψ is indicative of the presence of a manoeuvre only in high-intensity cases. For low- and medium-intensity manoeuvres, they are, in principle, indistinguishable from process noise, unless the manoeuvre happened at a long enough distance from the first radar measurement. The main cause of this is, besides the long gap without measurement, having less radar measurements; in the case of Sentinel 1-A, nine values were obtained as the pass after the manoeuvre is longer, whereas in the case of Swarm C, only five values are obtained.

6.2 Reachability Analysis Algorithm 1 Results.

Table 2 contains the results of Algorithm 1.

Case / Metric	MD $(\rho, \dot{\rho})$	PR (%)	MD (El,Az)	PR (%)	MD (All)	PR (%)
WoM	0,29	0	2,18	33	2,60	0
L-12h	1,54	8	1,66	13	2,22	0
L-6h	1,16	0	1,52	7	1,96	0
L-2h	1,35	0	2,10	30	2,16	0
M-12h	3,17	59	2,15	32	3,97	18
M-6h	4,66	81	0,97	0	4,81	39
M-2h	4,32	77	2,29	36	4,80	38
H-12h	23,48	100	3,61	67	23,53	100
H-6h	30,37	100	4,44	78	30,38	100
H-2h	12,27	100	1,23	0	12,44	97

Table 2. Sentinel 1A Reachability analysis with Algorithm 1 and probability from MD using (22). WoM=without manoeuvre, L=low, M=medium, H=high.

In the table, the Mahalanobis distance (MD) has been computed considering only range-range rate (column 2), El-Az (column 4) and all data (column 6). Based on the MD, a probability measure has been computed based on the MD being distributed as a χ^2distribution function

with as many degrees of freedom (n) as variables. Thus, the number PR (which is a possible estimation of the probability of manoeuvre) is computed as follows:

$$PR = \max\{0, 2(\chi^2(MD; n) - 0.5\}. \qquad (22)$$

This way, if the MD has a probability of 50% or less of occurring, it is assumed that there is no manoeuvre, to reduce false positives. If the MD has a probability of more than 50% of happening, then one subtracts 50 from the probability and multiplies it by two; if one gets, e.g., a probability of a certain MD of 80%, the probability of manoeuvre would be 60%.

From the results, several conclusions can be drawn:

- In general, using only range and range rate is more sensitive in more cases; using elevation and azimuth can induce false positives.
- All high- and medium-intensity manoeuvres are detected.
- Low-intensity manoeuvres are usually not detected.
- The distance to the radar measurement does not seem to affect these results.

The results can be inspected visually in Figure 9. Note that due to the propagation "stretching" the orbit uncertainty in the range-range rate plane, it is hard to verify if measurements belong to the confidence region, except in high-intensity cases. In the Swarm C case (not shown), only high-intensity manoeuvres are detected, with varying success for medium-intensity manoeuvres.

6.3 Reachability Analysis Algorithm 2 Results.

It is not immediate to use Algorithm 2 to detect manoeuvres, since it produces a distribution of ΔV that might be hard to interpret; thus, a basic Monte Carlo simulation of the case with no-manoeuvres has been carried out to find the distribution in the non-manoeuvred case. This is shown in Figure 7. The Monte Carlo simulation allows to derive a "mean distribution" as well as a distribution at a 2-sigma distance from the mean, which is helpful to avoid false positives. The percentiles 10%, 50% and 80% are computed for these two distributions as well as for all the simulations to derive several possible different metrics for the probability of manoeuvre, as follows. P1M and P1D compare the percentile 10% of the resulting ΔV with the mean (respectively, 2-sigma) non-manoeuvred distribution. The algorithm computes the probability p of the resulting ΔV to be below this non-manoeouvred value, then:

$$P1 = \max\{0, 0.1(0.1 - p)\}. \qquad (23)$$

This way, if p is above 10% the probability becomes zero and if it is below 10, the difference is multiplied by 10 (thus, having zero probability would represent a 100% probability of manoeuvre). P5M and P5D are computed similarly for the 50% percentile. P8M and P8D are computed similarly for the 80% percentile.

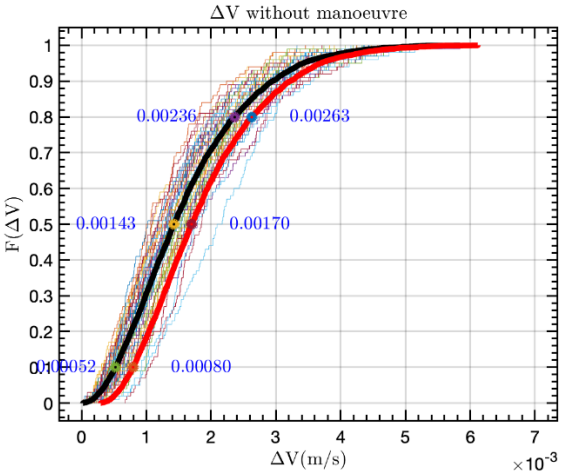

Figure 7. Monte Carlo analysis of non-manoeuvred results of Algorithm 1 (Sentinel 1-A case). Black: mean distribution. Red: mean plus 2-sigma distribution.

From the results in Table 3, some conclusions are drawn:

- Algorithms detect all high- and (except P8M and P8D) medium-intensity manoeuvres.
- P1M is the most sensitive algorithm being able to detect even some low-intensity manoeuvres. However, it has a non-negligible rate of false positives (a false positive is defined as a non-manoeuvred case from the Monte Carlo simulation being detected with $p \geq 50\%$).
- P1D is also quite sensitive and, even though it fails in detecting some manoeuvres that P1M detects, it reduces the number of false positives.
- Other metrics are worse than P1M and P1D.

The computed CDFs can be inspected visually in Figure 10. In the Swarm C case (not shown), only high-intensity manoeuvres are detected, with varying success for medium-intensity ones. As in Section 6.1, The main causes are long gaps without measurement and having less radar measurements right after the manoeuvre.

7 CONCLUSIONS AND FUTURE WORK

Several methods for the detection of manoeuvres in LEO from radar data have been presented, based on UKF, attributable theory and reachability analysis. Simulation results using OREKIT show that the filter does not detect manoeuvres unless they are rather intense, whereas the reachability approach is more sensitive at the price of longer computation times. As a next step, the filter and reachability approaches will be unified, to improve detection and orbit estimation. The aim is to have these algorithm integrated in the S3T Cataloguing System in order to provide routine automatic manoeuvre detection capabilities to the system in the future.

Case/ Metrics	P1M (%)	P5M (%)	P8M (%)	P1D (%)	P5D (%)	P8D (%)
FP	10	1	0	3	0	0
L-12h	100	72	0	70	40	0
L-6h	100	42	0	50	0	0
L-2h	0	0	0	0	0	0
M-12h	100	96	0	100	84	0
M-6h	100	100	95	100	100	95
M-2h	100	98	0	100	96	0
H-12h	100	100	100	100	100	100
H-6h	100	100	100	100	100	100
H-2h	100	100	100	100	100	100

Table 3. Sentinel 1-A probability of manoeuvre. FP=false positives, L=low, M=medium, H=high.

In addition, validation of all the algorithms will be carried out with real tracks from S3TSR [1], the Spanish surveillance radar developed, installed and validated by Indra with the funding of the Spanish Government under technical and contractual management of ESA on behalf of Centro de Desarrollo Tecnológico e Industrial (CDTI). Manoeuvre information and ephemerides will be obtained from ESA/ESOC and DLR/GSOC to assess the results. The simulation results predict that the measurements provided by the actual version of S3TSR will allow for the detection of sufficiently intense manoeuvres of the LEO objects that the radar can observe.

8 REFERENCES

1. Gomez, R., Salmerón, J. M. V., Besso, P., Alessandrini, M., Pinna, G. M., & Prada, M. A. R. (2019). *Initial Operations of the Breakthrough Spanish Space Surveillance and Tracking Radar (S3TSR) in the European Context*. 1st ESA NEO and Debris Detection Conference, Darmstadt, Germany.
2. Goff, G. M. (2015). *Orbit Estimation of Non-Cooperative Maneuvering Spacecraft*. PhD Thesis. Ohio, USA.: USAF Institute of Technology.
3. Tapley, B. D., Schutz, B. E. & Born, G. H. (2004). *Statistical Orbit Determination*. Elsevier.
4. Li, X. R. & Jilkov, V. P. (2005). Survey of Maneuvering Target Tracking. Part V: Multiple-Model Methods. *IEEE Trans Aerosp Electron Sys*, **41**(4), 1255-1321.
5. Woodburn, J., Carrico, J. & Wright, J. R. (2003). Estimation of Instantaneous Maneuvers Using a Fixed Interval Smoother. *Advances in the Astronautical Sciences*, **116**, 243-260.
6. Guang, Z., Xingzi, B., Hanyu, Z. & Bin, L. (2018). Non-Cooperative Maneuvering Spacecraft Tracking via a Variable Structure Estimator. *Aerospace Science and Technology*, **79**, 352-363.
7. Ye, L., Hua, Z., Chuankai, L., Jianfeng, C. & Junkui, W. (2020). Maneuver Detection and Tracking of a Space Target Based on a Joint Filter Model. *Asian Journal of Control, 1-13.*
8. Goff, G. M., Showalter, D., Black, J. T. & Beck, J. A. (2015). Parameter Requirements for Noncooperative Satellite Maneuver Reconstruction Using Adaptive Filters. *J Guid Control Dyn*, **38**(3), 361-374.
9. Goff, G. M., Black, J. T. & Beck, J. A. (2015). Tracking Maneuvering Spacecraft with Filter-Through Approaches Using Interacting Multiple Models. *Acta Astronautica*, **114**, 152-163.
10. Holzinger, M. & Scheeres, D. (2009). Reachability Analysis Applied to Space Situational Awareness. *In Advanced Maui Optical and Space Surveillance Technologies Conference*, 395-404.
11. Sanchez, J. C., Louembet, C., Gavilan, F. & Vazquez, R. (2019). An Event-Triggered Predictive Controller for Spacecraft Rendezvous Hovering Phases. *IFAC-PapersOnLine*, **52**(12), 97-102.
12. Kurzhanski, A. B. & Varaiya, P. (2000). Ellipsoidal Techniques for Reachability Analysis. *In International Workshop on Hybrid Systems: Computation and Control* (pp. 202-214).
13. Scott, J. K. & Barton, P. I. (2013). Bounds on the Reachable Sets of Nonlinear Control Systems. *Automatica*, **49**(1), 93-100.
14. Girard, A. (2005). Reachability of Uncertain Linear Systems Using Zonotopes. *In International Workshop on Hybrid Systems: Computation and Control* (pp. 291-305). Springer, Berlin, Heidelberg.
15. Jain, A., Guého, D., Singla, P. & Akella, M. (2019). Stochastic Reachability Analysis for the Hypersonic Re-Entry Problem. *In 29th AAS/AIAA Space Flight Mechanics Meeting*, 2019 (pp. 2455-2476).
16. Armellin, R., Di Lizia, P., Bernelli-Zazzera, F. & Berz, M. (2010). Asteroid Close Encounters Characterization Using Differential Algebra: The Case of Apophis. *Celestial Mechanics and Dynamical Astronomy*, **107**(4), 451-470.
17. Perez, D., Masdemont, J. J. & Gomez, G. (2013). Jet Transport Propagation of Uncertainties for Orbits Around the Earth. *64th International Astronautical Congress*, Beijing. China.

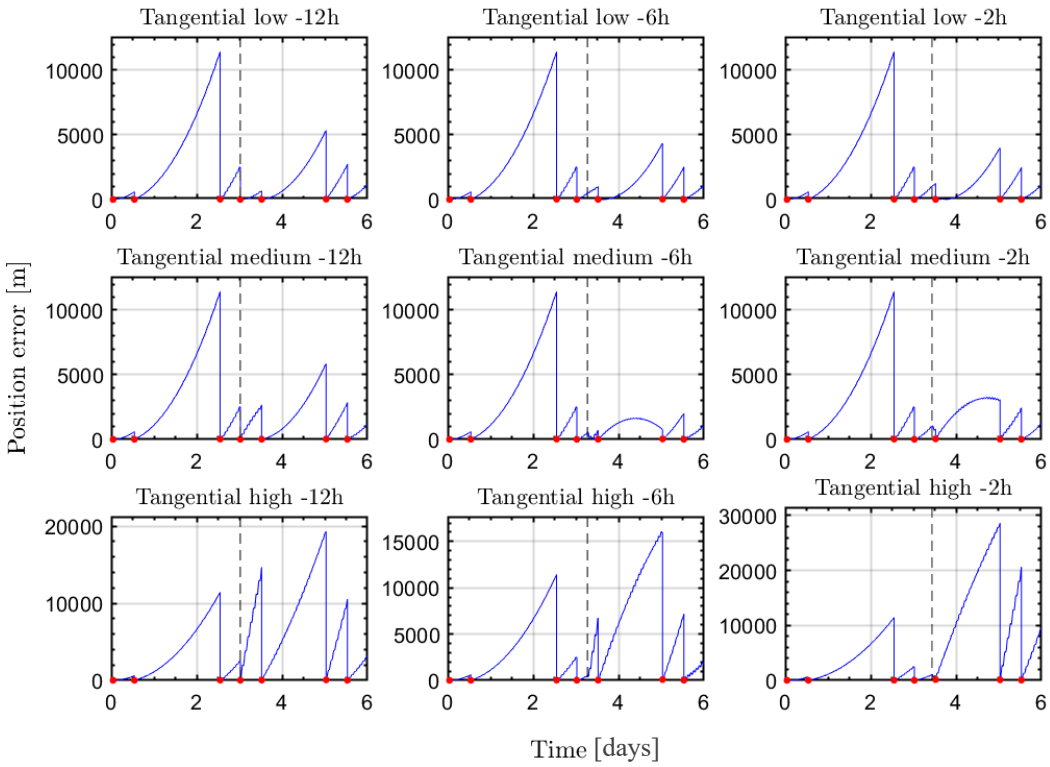

Figure 8. Position error with respect to "real" orbit for Sentinel-1A manoeuvred scenarios. Red dots indicate the mismatch between measurements and the predicted state after the filter update.

18. Vananti, A., Schildknecht, T., Siminski, J., Jilete, B., & Flohrer, T. (2017). Tracklet-Tracklet Correlation Method for Radar and Angle Observations. *In Proc. 7th European Conference on Space Debris*, Darmstadt, Germany (pp. 18-21).

19. Reihs, B., Vananti, A., Schildknecht, T., Siminski, J. & Flohrer, T. (2020). Application of Attributables to the Correlation of Surveillance Radar Measurements. *arXiv preprint arXiv:2009.07559*.

20. Singh, N., Horwood, J. T. & Poore, A. B. (2012). Space Object Maneuver Detection via a Joint Optimal Control and Multiple Hypothesis Tracking Approach. *In Proceedings of the 22nd AAS/AIAA Space Flight Mechanics Meeting*, **143**, pp. 2012-159). San Diego, CA.

21. Holzinger, M. J., Scheeres, D. J. & Alfriend, K. T. (2012). Object Correlation, Maneuver Detection, and Characterization Using Control Distance Metrics. *J Guid Control Dyn*, **35**(4), 1312-1325.

22. Siminski, J., T. Flohrer, and Thomas Schildknecht. (2017). Assessment of Post-Maneuver Observation Correlation Using Short-Arc Tracklets. *Journal of the British Interplanetary Society* **70**, 63-68.

23. Julier, S. J. & Uhlmann, J. K. (1997). New Extension of the Kalman Filter to Nonlinear Systems. *In Signal processing, sensor fusion, and target recognition*, 3068, 182-193.

24. Wan, E. A. & Van Der Merwe, R. (2000). The Unscented Kalman Filter for Nonlinear Estimation. *In Proceedings of the IEEE 2000 Adaptive Systems for Signal Processing, Communications, and Control Symposium*, 153-158.

25. OREKIT: Spaceflight Dynamics Library (2016). http://orekit.org.

26. Poore, A. B., Aristoff, J. M., Horwood, J. T., Armellin, R., Cerven, W. T., Cheng, Y. & Jones, B. A. (2016). *Covariance and Uncertainty Realism in Space Surveillance and Tracking*. Numerica Corporation Fort Collins United States.

27. Russell, J.C. & D'Souza, C.N. (2018). *Navigation Filter Best Practices.* NASA Technical Publication 2018-219822, chapter 2, pp. 15-25.

28. Andre, A. & Maisonobe, L. (2016). Automatic Differentiation for Propagation of Orbit Uncertainties on OREKIT. *Stardust Conference 2016*, at ESTEC Noordwijk, Netherlands.

29. Andersson, J. A., Gillis, J., Horn, G., Rawlings, J. B., & Diehl, M. (2019). CasADi: A Software Framework for Nonlinear Optimization and Optimal Control. *Math. Prog. Comp.* **11**(1), 1-36.

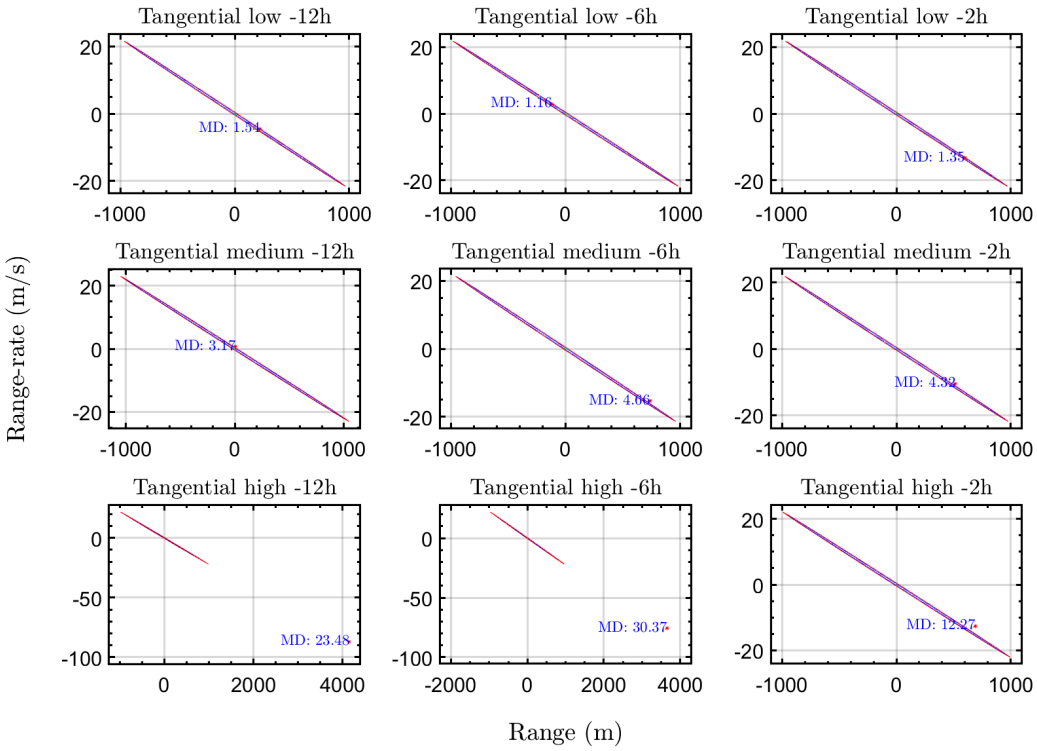

Figure 9. Reachability results (Algorithm 1) for Sentinel 1A manoeuvre, Range vs Range-rate.

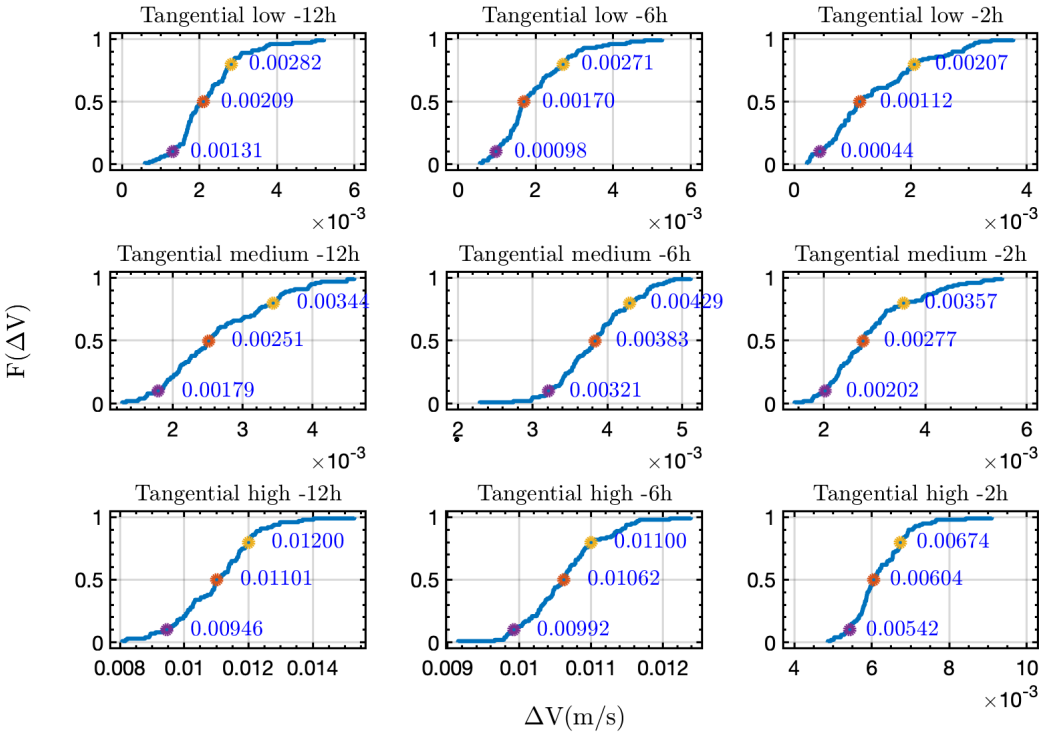

Figure 10. Reachability results (Algorithm 2) for Sentinel 1-A.